View metadata, citation and similar papers at core.ac.uk

brought to you by CORE

provided by James Madison University

James Madison University
JMU Scholarly Commons

Physics and Astronomy | College of Science and Mathematics

2-1-2012

Effects of Metallic, Semiconducting, and Insulating Substrates on the Coupling Involving Radiative Polaritons in Thin Oxide Films

Anita J. Vincent-Johnson
James Madison University

Kyle A. Vasquez
James Madison University

Giovanna Scarel
James Madison University

James S. Hammonds Jr.
Howard University

Mathieu Francoeur
University of Utah

Follow this and additional works at: http://commons.lib.jmu.edu/paa

Part of the Atomic, Molecular and Optical Physics Commons

Recommended Citation
Vincent-Johnson, A. J., Vasquez, K. A., Scarel, G., Hammonds, J. S., & Francoeur, M. (2012). Effects of Metallic, Semiconducting, and Insulating Substrates on the Coupling Involving Radiative Polaritons in Thin Oxide Films. Applied Spectroscopy, 66(2), 188197. doi:10.1366/11-06489

This Article is brought to you for free and open access by the College of Science and Mathematics at JMU Scholarly Commons. It has been accepted for inclusion in Physics and Astronomy by an authorized administrator of JMU Scholarly Commons. For more information, please contact dc_admin@jmu.edu.

applied
spectroscopy

Effects of Metallic, Semiconducting, and Insulating Substrates on the Coupling Involving Radiative Polaritons in Thin Oxide Films

ANITA J. VINCENT-JOHNSON, KYLE A. VASQUEZ, GIOVANNA SCAREL,* JAMES S. HAMMONDS, Jr., and MATHIEU FRANCOEUR

Department of Physics and Astronomy (A.J.V.-J., G.S.), and Department of Chemistry and Biochemistry, James Madison University, Harrisonburg, Virginia 22807 (K.A.V.); Department of Mechanical Engineering, Howard University, Washington, D.C. 20059 (J.S.H.); and Department of Mechanical Engineering, University of Utah, Salt Lake City, Utah 84112 (M.F.)

Official Publication of the Society for Applied Spectroscopy

Effects of Metallic, Semiconducting, and Insulating Substrates on the Coupling Involving Radiative Polaritons in Thin Oxide Films

ANITA J. VINCENT-JOHNSON, KYLE A. VASQUEZ, GIOVANNA SCAREL,* JAMES S. HAMMONDS, JR., and MATHIEU FRANCOEUR

Department of Physics and Astronomy (A.J.V.-J., G.S.), and Department of Chemistry and Biochemistry, James Madison University, Harrisonburg, Virginia 22807 (K.A.V.); Department of Mechanical Engineering, Howard University, Washington, D.C. 20059 (J.S.H.); and Department of Mechanical Engineering, University of Utah, Salt Lake City, Utah 84112 (M.F.)

Through simulations, this work explores the effects of conducting, semiconducting, and insulating substrates on the absorption of infrared radiation by radiative polaritons in oxide layers with thicknesses that range from 30 nm to 9 μm. Using atomic layer deposition, oxide layers can be formed in the nanometer scale. Our results suggest that the chemistry and conductivity of the substrate determine the amount of absorption by radiative polaritons in oxide layers thinner than the skin depth. The effects of the chemistry and conductivity of the substrate are especially effective for oxide films thinner than about 250 nm, which we label as the *substrate sensitive thickness* of the oxide film.

Index Headings: **Infrared spectroscopy; Radiative polaritons; Atomic layer deposition; Thin oxide films.**

INTRODUCTION

Electromagnetic radiation interacts with matter in different ways depending upon frequency. High-frequency γ and X-ray photons interact through the Compton effect, or Compton scattering, while ultraviolet (UV) and visible photons interact through the photoelectric effect. Visible light, in addition, participates in many chemical reactions of biological importance, such as photosynthesis. Infrared (IR) radiation, on the other hand, interacts with matter via coupling to dynamic dipoles. In particular, in inorganic solid and ionic crystals IR photons can interact and couple with the collective lattice vibrations called phonons, thus exciting polaritons.[1,2] Understanding the interaction of radiation with matter is crucial from a fundamental and a practical point of view. Indeed, radiation–matter interactions are at the basis of energy conversion devices such as solar photovoltaics. Presently, photovoltaic cells are used to convert absorbed visible photons into usable energy. There is also emerging interest in capturing IR radiation for energy conversion,[3] thermal photovoltaics,[3,4] and enhanced thermal transport at interfaces.[3,5–7] Such applications have led to the study of polaritons,[1,2] which form when IR photons couple with phonons present in dielectric materials featuring ionic bonds. Multiple types of polaritons exist, including surface phonon polaritons (SPPs)[3–5] and radiative polaritons (RPs).[1,2]

This work focuses on RPs in thin oxide films. The effects of the chemistry and conductivity of the oxide film substrate on the interaction between IR radiation and planar thin oxide films have been discussed in the literature only to a limited extent. Authors have studied films on metal substrates,[8–13] semiconducting substrates,[14–19] and insulating substrates.[20–22] A comparison of the effects of the conductivity of different metal substrates can also be found.[9,10] In addition, there is experimental and simulated data available for oxide layers less than 1 μm thick, where the IR optical properties are sensitive to the chemistry and conductivity of the substrate.[19,22] However, there has been no comprehensive study that examines how variations in substrate chemistry and conductivity impact IR radiation absorption in thin oxide films. Oxide films less than 1 μm thick are of technological relevance (e.g., in microelectronics)[23] and can be formed with high quality by utilizing, e.g., atomic layer deposition (ALD).[24] Therefore, knowing the effects of the chemistry and conductivity of the substrate on the oxide film's ability to absorb IR radiation might become of compelling importance in future applications. It is important to point out that oxide films deposited by ALD, especially Al_2O_3, are very uniform in thickness and have low roughness (less than 10% of the film thickness).[24]

This work investigates numerically the absorption of IR radiation in thin planar oxide films on metallic, semiconducting, and insulating substrates. The absorption of the IR radiation is related to the excitation of RPs, as in the theory by Kliewer et al.[2,25] This theory, which originally considers simple cubic oxides with one couple of longitudinal (ω_{LO}) and transverse (ω_{TO}) optical phonon frequencies, will be extended here to oxides characterized by more than one couple of ω_{LO} and ω_{TO} frequencies. Such oxides, despite being very common, are neglected in the present literature on RPs. Their complex crystalline structure is reflected in their dielectric function (ε_{oxide}), as will be discussed.

An RP is a mixed excitation resulting from the strong coupling between the TO phonons and the IR photon field in dielectric (oxide or semiconductor) layers.[2] Unlike non-radiative polaritons,[1] RPs have a phase velocity such that $(\omega/|\mathbf{k}|)^2 > (c)^2$,[2] where ω is the angular frequency, $|\mathbf{k}|$ is the modulus of the wave-vector, and c is the speed of light. A consequence of this physical paradox is that the RPs leak energy to the surrounding space.[2] The RP frequency is therefore complex: $\omega = \mathrm{Re}(\omega) + i\,\mathrm{Im}(\omega)$, where $\mathrm{Re}(\omega)$ is the central frequency, and $\mathrm{Im}(\omega)$ gives the spread in frequency of the RP.[2,19] The value of $2|\mathrm{Im}(\omega)|$ is the inverse of the lifetime (or damping)[2,19] of the RP, which is of the order of picoseconds. Since the wave vector $|\mathbf{k}|$ is also complex,[2,19] the dispersion relations of RPs are represented by plotting $\mathrm{Re}(\omega)$ and $\mathrm{Im}(\omega)$ versus the angle of incidence θ_0 of the IR radiation, not versus $\mathbf{k}$. This procedure is possible because the

Received 29 September 2011; accepted 10 November 2011.
* Author to whom correspondence should be sent. E-mail: scarelgx@jmu.edu.
DOI: 10.1366/11-06489

0003-7028/12/6602-0188$2.00/0
© 2012 Society for Applied Spectroscopy

relationship between **k** and θ_0 is, e.g., in the *x*-axis, $k_x = |\mathbf{k}| \sin \theta_0$.[2,19] Radiative polaritons appear at frequencies above or below the ω_{LO} and ω_{TO} frequencies. The frequency and number of RPs that the substrate can support depend on the thickness *d* of the dielectric layer.[2] For dielectric layers on a metallic substrate, only half of all possible RPs exist because the boundary conditions eliminate those RPs that are accompanied by electric fields parallel to the metal surface.[2,25]

In this work, the simulations are performed utilizing a well-established method based on Fresnel's equations extended to multilayer systems through a system of transfer matrices. These matrices can efficiently describe the refraction and reflection of IR radiation incident on multilayer systems[26] at various values of incidence angle θ_0[14] and oxide film thickness *d*,[15] and for various geometries.[20] Here, we examine the absorption of IR radiation by γ-Al_2O_3 and anatase-TiO_2 with dielectric functions $\varepsilon_{Al_2O_3}$ and ε_{TiO_2}, respectively.[27] The dielectric functions depend not only on oxide chemical composition, but also on its crystalline structure; e.g., ε_{TiO_2} is different for anatase and rutile TiO_2.[20,28] The angular dependence for absorption is investigated in the 0 to 81° range.[11,25] The dispersion relations of γ-Al_2O_3 films will be discussed in a separate report.

SIMULATION PROCEDURE

This work considers thin oxide layers with $d < \lambda_{IR}$, where *d* is the oxide film thickness and λ_{IR} is the wavelength of the IR radiation (15–30 μm). According to the description of IR absorption by oxide films in terms of RP coupling given by Kliewer et al.,[2,25] in thin oxide films, for $\mathrm{Re}(\omega) \geq \omega_{LO}$, only the 0TH type-RP exists. This RP is a solution to a tangent-type (T) of dispersion relation $-i\varepsilon_{oxide}(\beta_0/\beta) = \tan\beta d$. This kind of solution generates polarization vectors that always have a non-zero component normal at the oxide layer. In the above equation, $\beta_0 = \sqrt{(\omega^2/c^2) - k_x^2}$, and $\beta = \sqrt{\varepsilon_{oxide}(\omega^2/c^2) - k_x^2}$, where ε_{oxide} is the dielectric function of the oxide layer. The 0TH type-RP has $\mathrm{Re}(\omega) \geq \omega_{LO}$, and it is labeled with H to emphasize that it is a high-frequency RP.[2] On the other hand, the 2TL and 3CL type-RPs are the solutions of a tangent- and a cotangent-type (C) of dispersion relation, respectively. The cotangent-type dispersion relation is $i\varepsilon_{oxide}(\beta_0/\beta) = \cot\beta d$, and its solutions generate polarization vectors whose component normal to the oxide layer surface is always zero. The 2TL and 3CL type-RPs have $\mathrm{Re}(\omega) \leq \omega_{TO}$. These RPs are labeled with L, to emphasize that they are low-frequency RPs.[2] In summary, three types of RPs are excited in oxide films with thicknesses $d \leq 0.1\ \lambda_{IR}$,[2,25] and these RPs are assumed to be responsible for the absorption of IR radiation: the 0TH,[2] appearing at $\mathrm{Re}(\omega) \geq \omega_{LO}$, and the 2TL/3CL,[2] appearing at $\mathrm{Re}(\omega) \leq \omega_{TO}$. The optical properties of oxide films have been discussed in terms of RPs by various authors.[8,12,13,18,29–31]

The simulations apply to a four-layer system represented in Fig. 1, where it is assumed that the surfaces are perfectly smooth and parallel, consisting of air (layer 1), oxide film (layer 2), substrate (layer 3), and air (layer 4). The IR radiation illuminates the sample at an angle of incidence θ_0 and changes its direction of propagation according to Snell's law, as schematically described in Fig. 1. The method by Hansen,[26] used to derive the IR transmittance (*T*) and reflectance (*R*) through the four layers, characterizes each layer *j* by a transfer matrix:

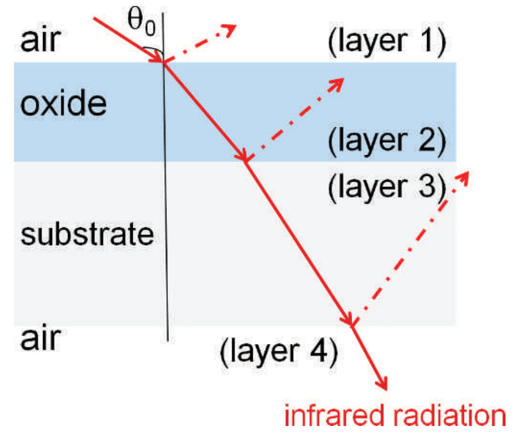

FIG. 1. Schematic of the four-layer system whose transmittance *T*, reflectance *R*, and absorptance *A* are studied using Fresnel's equation with the transfer matrix method formulated by Hansen.[26] Layer 1 is air, layer 2 is the oxide film, layer 3 is the substrate, and layer 4 is again air. The angle θ_0 is the incidence angle of the IR radiation on the planar surface, and the path of the IR radiation is traced by the arrowed straight lines. The dashed-dotted arrowed lines represent the reflected IR radiation.

$$M_j = \begin{vmatrix} \cos\beta_j & -\dfrac{i}{p_j}\sin\beta_j \\ -ip_j\sin\beta_j & \cos\beta_j \end{vmatrix} \tag{1}$$

with $\beta_j = (2\pi/\lambda)d_jN_j\cos\theta_j$, where d_j, N_j, and θ_j are, respectively, layer thickness, refractive index, and orientation with respect to the IR radiation. The term *i* is the imaginary unit, $p_{jTE} = (N_j/\sqrt{\mu_j})\cos\theta_j$, and $p_{jTM} = (\sqrt{\mu_j}/N_j)\cos\theta_j$, where TE (transverse electric) and TM (transverse magnetic) denote the polarization of the IR radiation, and μ_j is the magnetic permeability of the layer. Transmittance (*T*), reflectance (*R*), and absorptance ($A = 100\% - T - R$) of thin γ-Al_2O_3 and anatase-TiO_2 films are all obtained as a percentage of the total IR radiation incident onto the planar oxide films. The IR radiation of interest for the present investigation is located in the low part of the middle-IR region (400–1800 cm^{-1}), where the relevant 0TH and 2TL/3CL type-RPs can experimentally be detected.

The dielectric constant for air (layers 1 and 4) is $\varepsilon_{air} = 1.00059 + i0.00004$,[32] where the imaginary part causes the absorption of IR radiation in air. The dielectric function $\varepsilon(\omega)_{Al_2O_3}$ for γ-Al_2O_3 (layer 2) is given by Eq. 2 and the parameters are listed in Table I:[33]

$$\varepsilon(\omega)_{Al_2O_3} = \varepsilon\infty \prod_{m=1}^{n} \frac{\omega_{LOm}^2 - i\omega\gamma_{LOm} - \omega^2}{\omega_{TOm}^2 - i\omega\gamma_{TOm} - \omega^2} \tag{2}$$

Here, *n* is the total number of oscillators, γ_{LOm} and γ_{TOm} are their damping factors, and $\varepsilon_\infty = Lim_{\omega\to\infty}\varepsilon(\omega)_{oxide}$. For anatase-$TiO_2$ (also layer 2), the dielectric function $\varepsilon(\omega)_{TiO_2}$ is given by the linear combination of the A_{2u} and the E_u symmetry contributions[34,35] as follows:

$$\varepsilon(\omega)_{TiO_2} = \frac{\varepsilon(\omega)_{A_{2u}} + 2\varepsilon(\omega)_{E_u}}{3} \tag{3}$$

The functions $\varepsilon(\omega)_{A_{2u}}$ and $\varepsilon(\omega)_{E_u}$ appear as Eq. 2, with the parameters reported in Table II.[35] As seen in Tables I and II, γ-

TABLE I. Type of RP, and frequencies (in cm^{-1}) plus damping factors of the phonons related to the RPs in γ-Al_2O_3.[33] These parameters are used in the IR spectra simulations. The value of ε_∞ is 2.91.[33]

Radiative polariton	Frequency (ω) [cm^{-1}] and related phonon	Damping factor (γ) [cm^{-1}]
-	357, TO1	72
2TL 3CL	536, TO2	101
-	744, TO3	56
-	807, TO4	43
-	403, LO1	79
-	669LO2	68
-	783, LO3	53
0TH	917, LO4	49

TABLE II. Type of RP, and frequencies (in cm^{-1}) plus damping factors of the phonons related to the RPs in anatase-TiO_2.[35] These parameters are used in the IR spectra simulations. The value of ε_∞ for the A_{2u} symmetry is 5.41, whereas the one for the E_u symmetry is 5.82.[35]

Radiative polariton	Frequency (ω) [cm^{-1}] and related phonon	Damping factor (γ) [cm^{-1}]
-	367, TO1 - A_{2u}	68
-	755, LO1 - A_{2u}	79
-	262, TO2 - E_u	36
-	366, LO2 - E_u	4.1
2TL 3CL	435, TO3 - E_u	32
0TH	876, LO3 - E_u	33

Al_2O_3 and anatase-TiO_2 have four and three TO and LO frequency couples (related by the Lyddane–Sachs–Teller relation), respectively. Previous reports[14,34] show that the strongly absorbing 0TH type-RPs, which we study in this work, are near the ω_{LO4} and ω_{LO3} frequencies for γ-Al_2O_3 and anatase-TiO_2, respectively. The 2TL/3CL type-RPs, on the other hand, appear near the ω_{TO2} and ω_{TO3} frequencies for γ-Al_2O_3 and anatase-TiO_2, respectively.[14,34]

Aluminum (Al), silicon (Si), and silicon dioxide (SiO_2) are selected as substrate materials (layer 3) of different conductivities and defined thicknesses. For a 10 μm thick Al substrate, the dielectric function is $\varepsilon_{A1} = 1 + (i2\sigma/\omega)$, with $\sigma = (\sigma_0/1 - 2i\pi\tau\omega c)$. Here, $\sigma_0 = 3.67 \times 10^{17}$ s^{-1} is the direct current electrical conductivity, and $\tau = 0.8 \times 10^{-14}$ s is the relaxation time. The Si substrate has the dielectric function $\varepsilon(\omega)_{Si} = 12.25 - i0.021$,[36] and a 0.5 μm thickness. A thicker Si substrate would introduce interference fringes that limit the observation of the features in the IR spectra.[37] For a 10 μm thick SiO_2 substrate, the dielectric function is also given by Eq. 2, with parameters from Kirk[39] summarized in Table III. The simulated spectra obtained in this work are the result of the interaction between oxide films and IR radiation that can be characterized as consisting of 50% TE and 50% TM polarized radiation.[39]

The classical skin depth is calculated as follows:[40,41]

$$\delta = \frac{1}{\alpha} = \frac{\lambda_{IR}}{2\pi} \frac{1}{\mathrm{Im}N(\omega)_{oxide}} \tag{4}$$

TABLE III. Type of RP, and frequencies (in cm^{-1}) plus damping factors of the phonons related to the RPs in SiO_2.[38] These parameters are used in the IR spectra simulations. The value of ε_∞ is 2.356.[38]

Radiative polariton	Frequency (ω) [cm^{-1}] and related phonon	Damping factor (γ) [cm^{-1}]
2TL 3CL	1072, TO1	30
0TH	1235, LO1	35

where α is the film absorption coefficient, and $\alpha = (c/\omega)\mathrm{Im}N(\omega)_{oxide}$. The thin oxide film refractive index is $N(\omega)_{oxide} = \sqrt{\varepsilon(\omega)_{oxide}}$, where $\varepsilon(\omega)_{oxide}$ is given by Eq. 2 for γ-Al_2O_3 and by Eq. 3 for anatase-TiO_2. Figure 2 plots δ versus frequency, which shows in Fig. 2a that $\delta = 4$ μm at ω_{LO4} and $\delta = 1.1$ μm at ω_{TO2} for γ-Al_2O_3, and in Fig. 2b that $\delta = 4.5$ μm at ω_{LO3} and $\delta = 0.6$ μm at ω_{TO3} for anatase-TiO_2.

RESULTS AND DISCUSSION

Figure 3 shows the simulated percent (%) absorptance spectra ($A = 100\% - T - R$) obtained for various film thicknesses from 50 nm to 3 μm at $\theta_0 = 30°$ and 60° for γ-Al_2O_3/Al, γ-Al_2O_3/Si, and γ-Al_2O_3/SiO_2. The ω_{LO4} and ω_{TO2} frequencies are indicated by the vertical lines. The 0TH and 2TL/3CL type-RPs appear near the ω_{LO4} and ω_{TO2} frequencies, respectively. In panels (c) and (f) of Fig. 3, additional vertical lines point out the ω_{LO} and ω_{TO} frequencies of SiO_2 (labeled LO_s and TO_s, respectively).[38] The 0TH and 2TL/3CL type-RPs for SiO_2 appear near these frequencies. The same sequence of spectra is illustrated in Fig. 4 for anatase-TiO_2 in a thickness range from 50 nm to 7 μm. The spectra in Figs. 3 and 4 indicate that the absorptance peaks at the ω_{LO4} and ω_{LO3} frequencies, corresponding to the 0TH type-RP, increase significantly by increasing the oxide film thickness and the IR radiation incidence angle θ_0. The angular dependence of the absorptance of the 0TH type-RP near the ω_{LO4} and ω_{LO3} frequencies is known as the Berreman effect.[11] Its thickness-dependent increase and the blue-shift in frequency is in agreement with the RPs behavior described by Kliewer et al.[2,25] Similar trends are also revealed in the reflectance and transmittance spectra, also in agreement with Kliewer et al.[25] (spectra not shown).

From Figs. 3 and 4 we infer that the thickness- and angle-dependence of the absorption of the 0TH and 2TL/3CL type-RPs is related to the chemistry and conductivity of the substrate (specifically Al, Si, and SiO_2). In addition, the results on the absorption by oxide films on the insulating SiO_2 substrate (Figs. 3c and 3f, and Figs. 4c and 4f) are largely affected by the 2TL/3CL and 0TH type-RPs of SiO_2, as already noted by Ahn et al.[21]

The 0TH and 2TL/3CL type-RPs absorptance dependence on thickness for γ-Al_2O_3 and anatase-TiO_2 films is illustrated in Figs. 5 through 8. Figure 5 shows the absorptance spectra of the 2TL/3CL type-RPs versus oxide film thicknesses near ω_{TO2} for γ-Al_2O_3/Al (a), γ-Al_2O_3/Si (b), and γ-Al_2O_3/SiO_2 (c) in 30 nm to 5 μm thick films, and near ω_{TO3} for anatase-TiO_2/Al (d), anatase-TiO_2/Si (e), and anatase-TiO_2/SiO_2 (f) in 30 nm to 9 μm thick films. The simulations were performed fixing the incidence angle θ_0 at 0°, 30°, 60°, and 81°. The data indicate

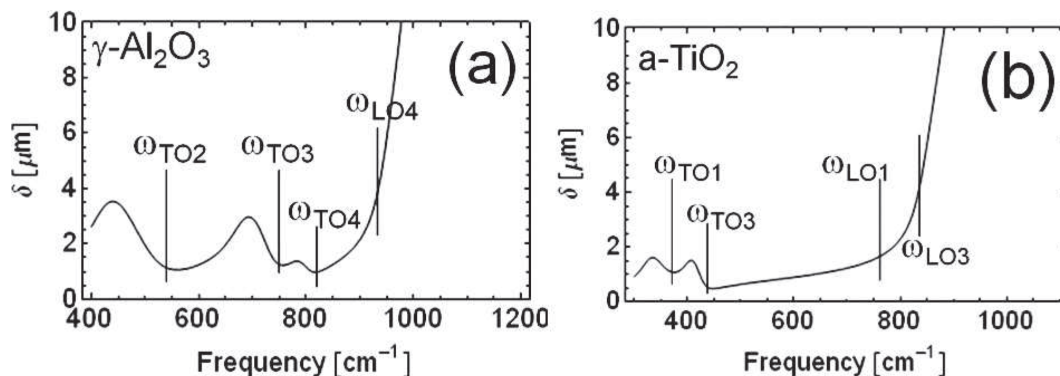

FIG. 2. The skin depth δ as a function of the angular frequency ω for γ-Al_2O_3 (**a**), and anatase-TiO_2 (**b**). The vertical lines indicate the location of the ω_{LO} and ω_{TO} frequencies of the oxides in the middle-IR region from 400 to 1800 cm^{-1}.

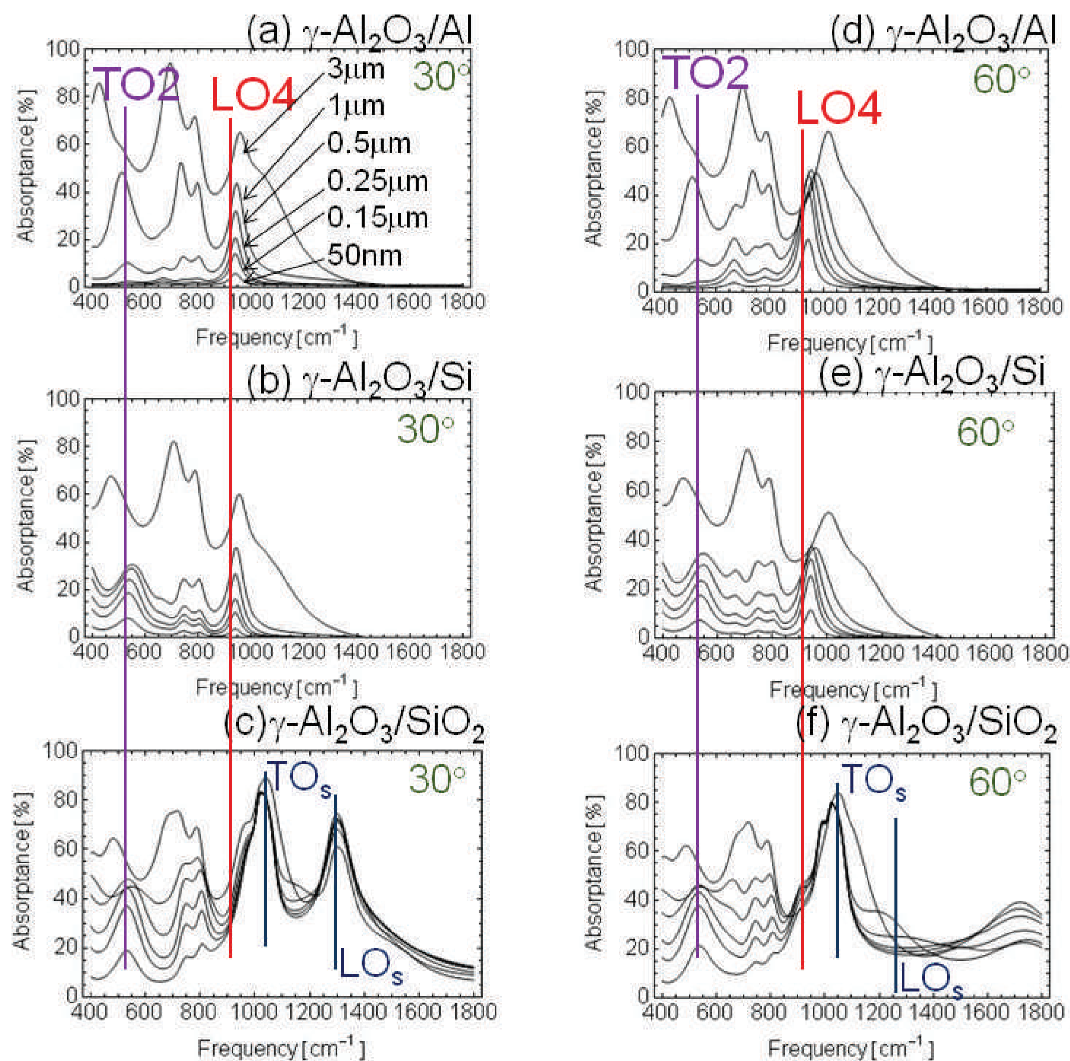

FIG. 3. Simulated absorptance spectra (100% − T − R) obtained for various film thicknesses at $\theta_0 = 30°$ for γ-Al_2O_3/Al (**a**), γ-Al_2O_3/Si (**b**), and γ-Al_2O_3/SiO_2 (**c**), and at $\theta_0 = 60°$ for γ-Al_2O_3/Al (**d**), γ-Al_2O_3/Si (**e**), and γ-Al_2O_3/SiO_2 (**f**). The vertical lines indicate the ω_{LO4} and ω_{TO2} frequencies. The 0TH and 2TL/3CL type-RPs are the peaks that appear near the ω_{LO4} and ω_{TO2} frequencies, respectively. In panels (**c**) and (**f**) additional vertical lines indicate the LO_s and TO_s frequencies of SiO_2.[38] The 0TH and 2TL/3CL type-RPs of SiO_2 are the peaks near the LO_s and TO_s frequencies, respectively. The oxide film thicknesses are labeled in panel (**a**), and the sequence is the same in all panels.

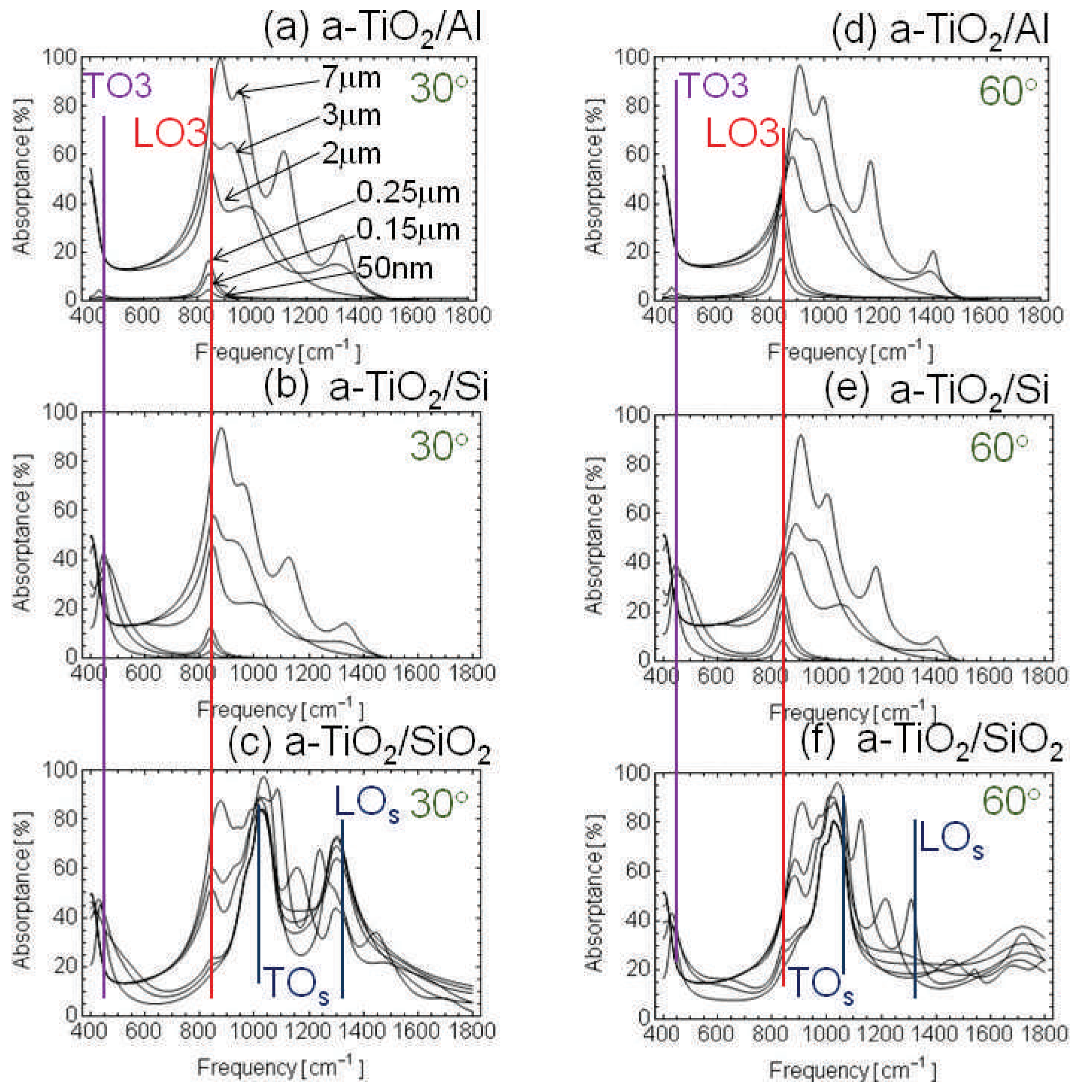

FIG. 4. Simulated absorptance spectra ($100\% - T - R$) obtained for various film thicknesses at $\theta_0 = 30°$ for anatase-TiO_2/Al (**a**), anatase-TiO_2/Si (**b**), and anatase-TiO_2/SiO_2 (**c**), and at $\theta_0 = 60°$ for anatase-TiO_2/Al (**d**), anatase-TiO_2/Si (**e**), and anatase-TiO_2/SiO_2 (**f**). The vertical lines indicate the ω_{LO4} and ω_{TO2} frequencies. The 0TH and the 2TL/3CL type-RPs are the peaks that appear near the ω_{LO4} and ω_{TO2} frequencies, respectively. In panels (**c**) and (**f**) additional vertical lines point out the LO_s and TO_s frequencies of SiO_2.[38] The 0TH and 2TL/3CL type-RPs of SiO_2 are the peaks near the LO_s and TO_s frequencies, respectively. The oxide film thicknesses are labeled in panel (**a**), and the sequence is the same in all panels.

that for $d > \delta$ the dependence of absorption by the 2TL/3CL type-RPs on oxide film thickness is not affected by the chemistry and conductivity of the substrates. For $d < \delta$, however, the absorption by the 2TL/3CL type-RPs differs depending upon substrate chemistry and conductivity but does not depend upon θ_0 (except when $\theta_0 > 80°$). These phenomena can readily be observed in Fig. 6, which displays the same data as in Fig. 5 for $d < 250$ nm. In Fig. 6 we observe that the 2TL type-RP does not absorb IR radiation for $d < 250$ nm in γ-Al_2O_3 and anatase-TiO_2 films on Al. This phenomenon derives directly from the model described by Kliewer et al.,[2,25] which predicts that ultra-thin dielectric layers on a metallic substrate only support 2TL type-RPs with very long lifetime, thus ultra-narrow band width, and therefore cannot be observed. Surprisingly, this effect of the substrate on the absorption is more pronounced for oxide films less than 250 nm thick, and this result was not predicted in the original theory by Kliewer et al.[2] These conclusions are only slightly affected by the different oxide chemistry and crystalline structure of γ-Al_2O_3 and anatase-TiO_2.

Figure 7 shows the simulated percent (%) absorptance spectra versus film thicknesses of the 0TH type-RP near ω_{LO4} for γ-Al_2O_3/Al (a), γ-Al_2O_3/Si (b), and γ-Al_2O_3/SiO_2 (c) in films from 30 nm to 5 μm thick, and near ω_{LO3} for anatase-TiO_2/Al (d), anatase-TiO_2/Si (e), and anatase-TiO_2/SiO_2 (f) in films from 30 nm to 9 μm thick. Also in this case the simulations were performed by fixing the angle of incidence θ_0 at 0°, 30°, 60°, and 81°. The data suggest that for $d > \delta$ the dependence of the absorption by the 0TH type-RP on the oxide film thickness is not affected by the chemistry and conductivity of the substrate. Instead, for $d < \delta$, the absorption of the 0TH type-RPs always increases with θ_0 (Berreman effect)[11] but in a different way depending upon the chemistry and conductivity of the substrate. The absorption increase with θ_0 is highly

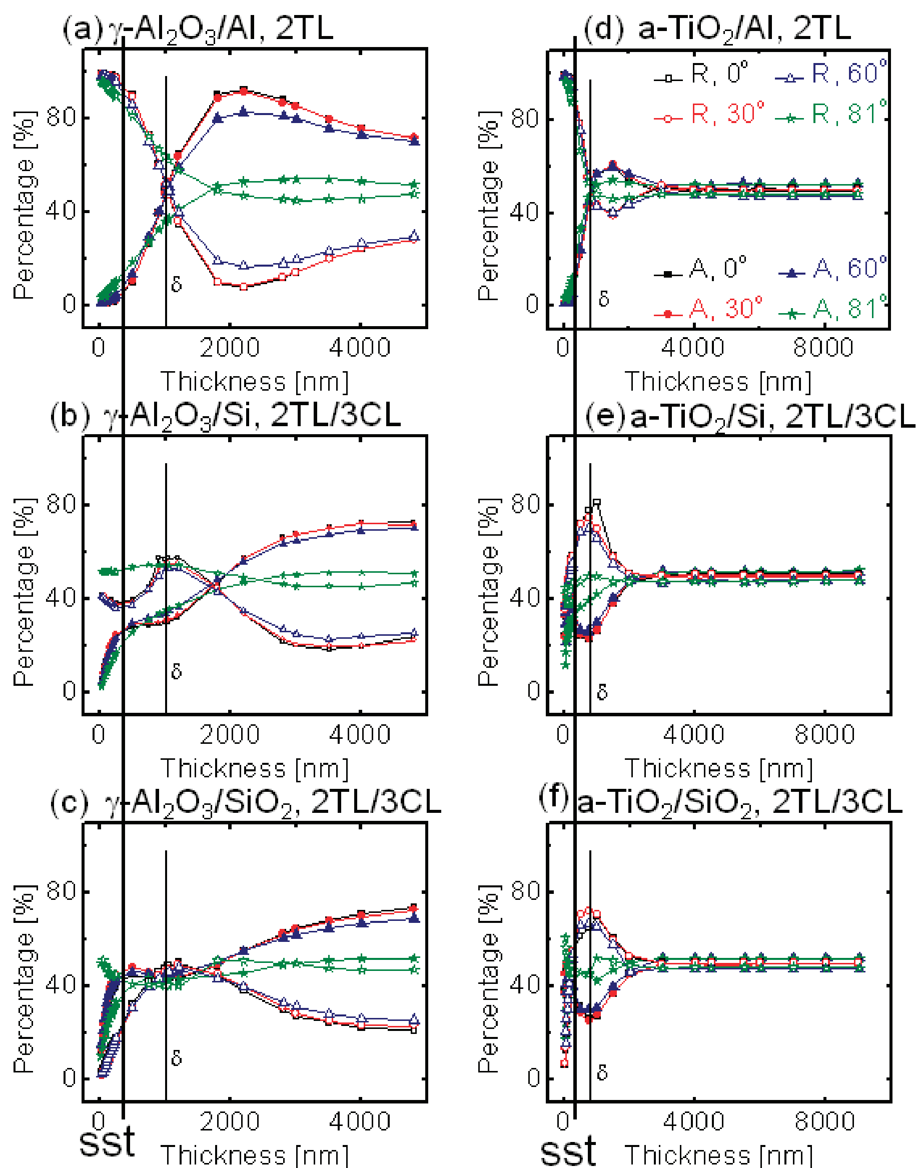

FIG. 5. Percent reflectance (R, empty symbols) and absorptance (A, filled symbols) versus oxide film thickness at $\theta_0 = 0°$ (squares), 30° (circles), 60° (triangles), and 81° (stars). For the 2TL/3CL type-RPs, the peaks near ω_{TO2} were considered for γ-Al_2O_3/Al (**a**), γ-Al_2O_3/Si (**b**), and γ-Al_2O_3/SiO_2 (**c**), whereas those near ω_{TO3} were considered for anatase (**a**)-TiO_2/Al (**d**), anatase-TiO_2/Si (**e**), and anatase-TiO_2/SiO_2 (**f**). The thick lines on the left of the graphs labeled "sst" represent the *substrate sensitive thickness*.

pronounced on the metallic substrate for all oxide thicknesses, especially below 250 nm, as can clearly be observed in Figs. 8a and 8d. For oxide films on semiconducting (Figs. 7b and 7e, and Figs. 8b and 8e) and insulating substrates (Figs. 7c and 7f, and Figs. 8c and 8f) the increased absorption as θ_0 increases, rises up to about 70°, and drops thereafter. Additionally, when dealing with insulating substrates, there is little variation of absorption with oxide film thickness, even for very thin films with $d \ll 250$ nm. In particular, our simulated spectra indicate that the Berreman effect appears only in oxide films with $d <$ 250 nm, especially for the films on a metallic substrate. This result was also not predicted in the theory by Kliewer et al.[2] However, in agreement with the Berreman effect[11] and the model described by Kliewer et al.,[2,14] we observe that the 0TH type-RPs do not absorb IR radiation at $\theta_0 = 0°$. These conclusions hold regardless of the oxide film chemistry considered. The reflection (R) data in Figs. 5 through 8 support the conclusions derived from the absorptance (A) data (spectra not shown).

Because ALD films are very uniform in thickness and smooth,[24] we do not expect film thickness deviations and interface roughness to interfere with the reported results.

SUMMARY AND CONCLUSIONS

We presented a study of the absorption of IR radiation by selected RPs in oxide films of variable thicknesses and orientations. The observed RPs are the 0TH-type, appearing near the ω_{LO4} frequency for γ-Al_2O_3 films and near the ω_{LO3} frequency for anatase-TiO_2, and the 2TL and 3CL-types, appearing near the ω_{TO2} frequency for γ-Al_2O_3 films and near the ω_{TO3} frequency for anatase-TiO_2. The Hansen method was

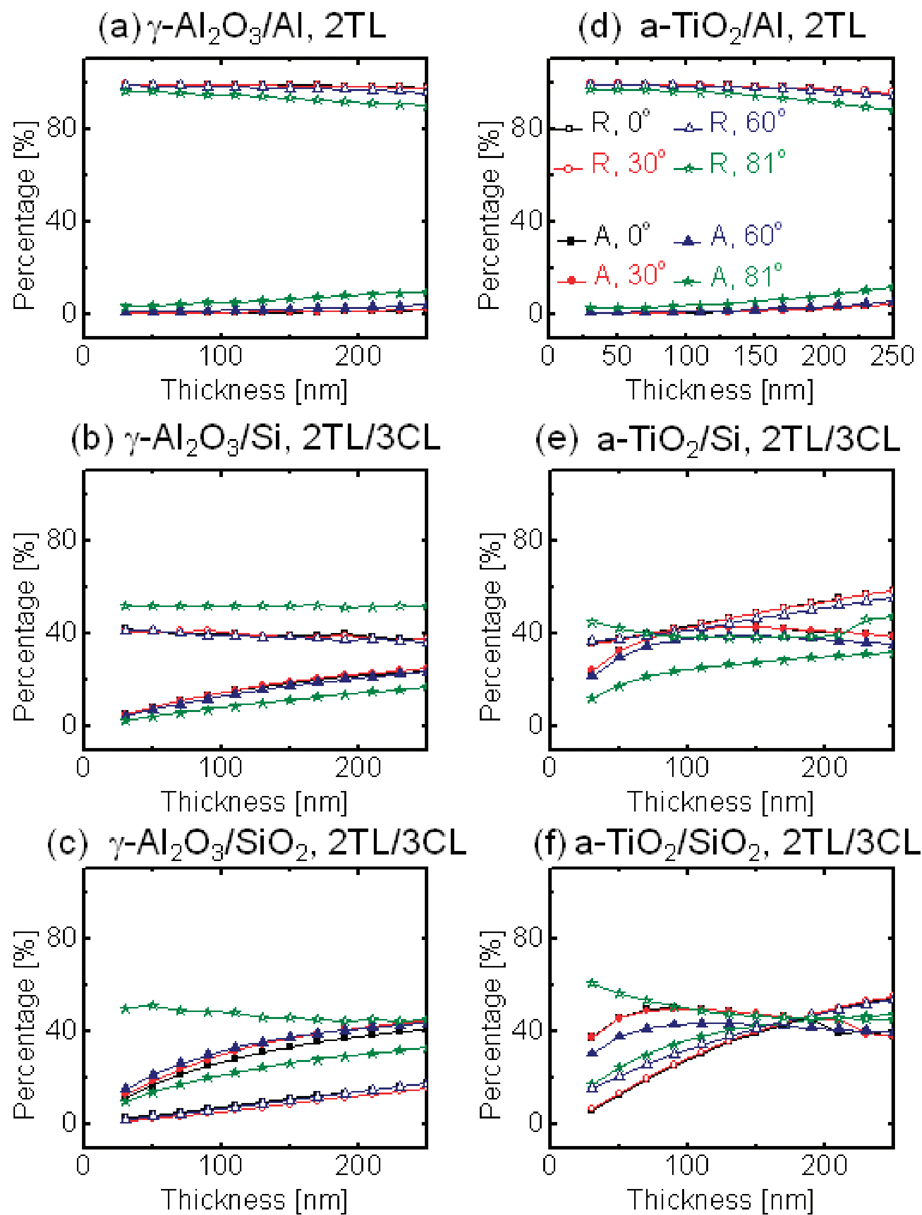

FIG. 6. Same as Fig. 5, zoomed into the oxide film thickness range between 30 and 250 nm.

used to simulate transmittance (T), reflectance (R), and absorptance ($100\% - T - R$) of thin γ-Al_2O_3 and anatase-TiO_2 films on Al, Si, and SiO_2.

The results presented in Figs. 5 through 8 show that the chemistry and the conductivity of the substrate determine the amount of absorption by the 0TH and 2TL/3CL type-RPs for oxide thicknesses less than the skin depth ($d < \delta$). In oxide layers with thickness $d > \delta$, there is no significant dependence of the RP absorption on the chemistry and conductivity of the substrate. This conclusion holds especially for the 2TL/3CL type-RPs.

Furthermore, the data in Figs. 7 and 8 indicate that the Berreman effect (i.e., the dependence of the absorption of the 0TH type-RP on the IR radiation incidence angle θ_0) is apparent in oxide films below about 250 nm, especially for oxide films on metallic substrates. The strength of absorption by the 0TH type-RP shows a dependence on film substrate previously unnoted, and not discussed in the original theory by Kliewer et al.[2,25] This phenomenon is, however, built into the Kliewer et al. formalisms describing the optical properties of the RPs.[14,25]

Finally, the data in Figs. 7 and 8 indicate that, in general, oxide chemistry, such as that of γ-Al_2O_3 and anatase-TiO_2 films on various substrates, only slightly affects the absorption of IR radiation by RPs, but substrate chemistry and conductivity can be noticeable in very thin oxide films with $d < 250$ nm. This finding was obtained by combining the Kliewer et al.[2,25] theory with the Fresnel's equations through the Hansen method[26] for simulating IR spectra of oxide films on substrates of any type of chemistry and conductivity. The upper limit thickness where the IR radiation interaction with the thin oxide film significantly depends on substrate chemistry and conductivity is labeled in Figs. 5

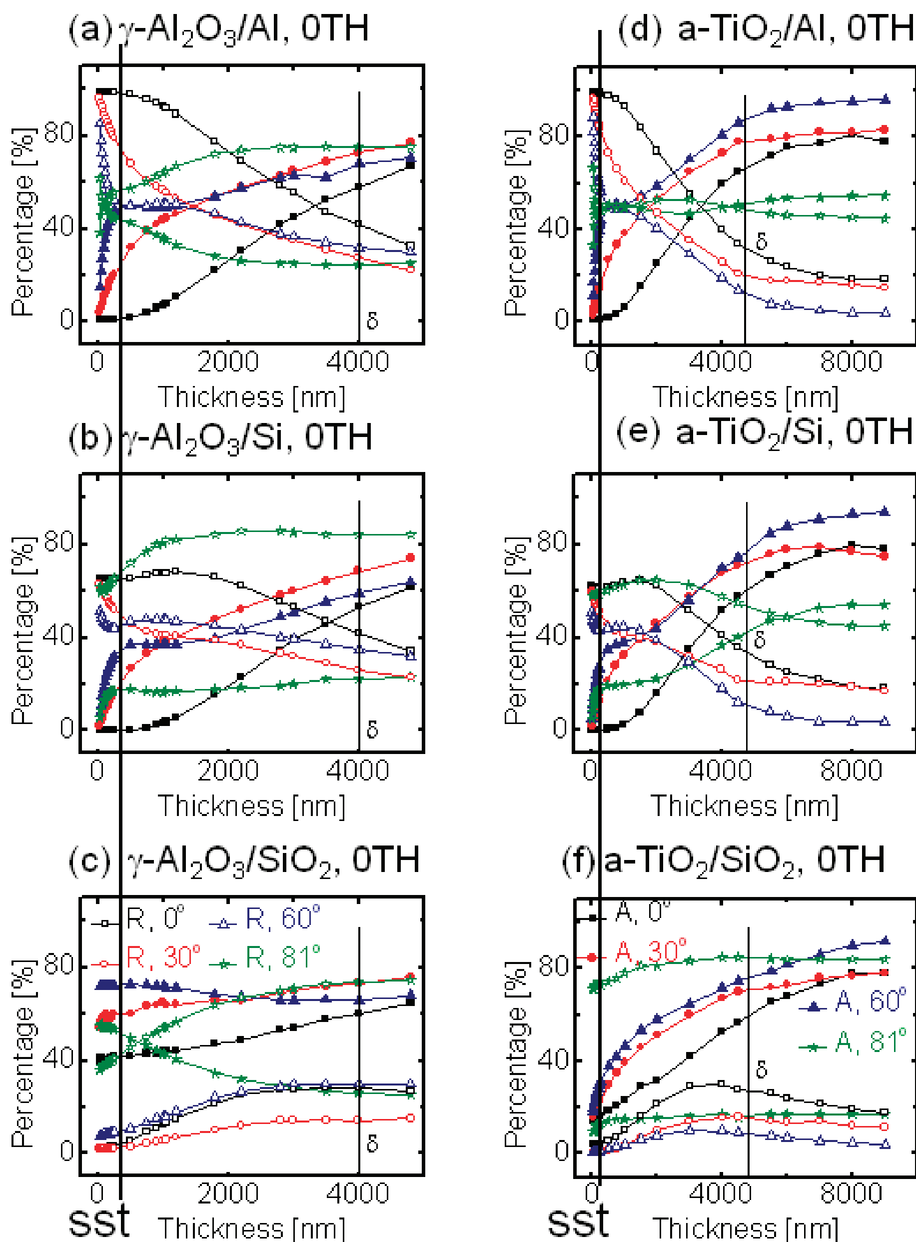

FIG. 7. Percent reflectance (*R*, empty symbols) and absorptance (*A*, filled symbols) versus oxide film thickness at $\theta_0 = 0°$ (square), 30° (circle), 60° (triangle), and 81° (star). For the 0TH type-RP, the peaks near ω_{LO4} were considered for γ-Al_2O_3/Al (**a**), γ-Al_2O_3/Si (**b**), and γ-Al_2O_3/SiO_2 (**c**), whereas that near ω_{LO3} was considered for anatase (**a**)-TiO_2/Al (**d**), anatase-TiO_2/Si (**e**), and anatase-TiO_2/SiO_2 (**f**). The thick lines on the left of the graphs labeled "sst" represent the *substrate sensitive thickness*.

and 7 as the *substrate sensitive thickness* (sst), or $d = 250$ nm.

In conclusion, our data show that (1) the chemistry and the conductivity of the substrate affect the IR radiation absorption by RPs in oxide films thinner than their IR skin depth δ, (2) the Berreman effect (the dependence of the absorption of the 0TH type-RP on the IR radiation incidence angle θ_0) occurs in oxide films less than about 250 nm thick, especially for oxide films on a metallic substrate, and (3) the chemistry of the oxide on various substrates only slightly affects the absorption by RPs, especially for oxide films thinner than 250 nm thick. Point (1) is supported by the behavior of the 0TH type-RP, where the increase in absorptance is higher in oxide films on Al, followed by those on Si and, lastly, on SiO_2. These results suggest that the chemistry and the conductivity of the substrate determine the amount of absorption by RPs in oxide layers thinner than the skin depth. In addition, the ability of an oxide film to interact with IR radiation is effective below the *substrate sensitive thickness*, which is about 250 nm regardless of oxide film chemistry.

ACKNOWLEDGEMENTS

This work was supported by the James Madison University Center for Materials Science, the James Madison University Department of Physics and Astronomy, the NSF-REU and Department of Defense ASSURE program (grant #0851367), the Research Corporation Science Department Development Grant 7957, and the Summer Research Grant 2011 from the James Madison

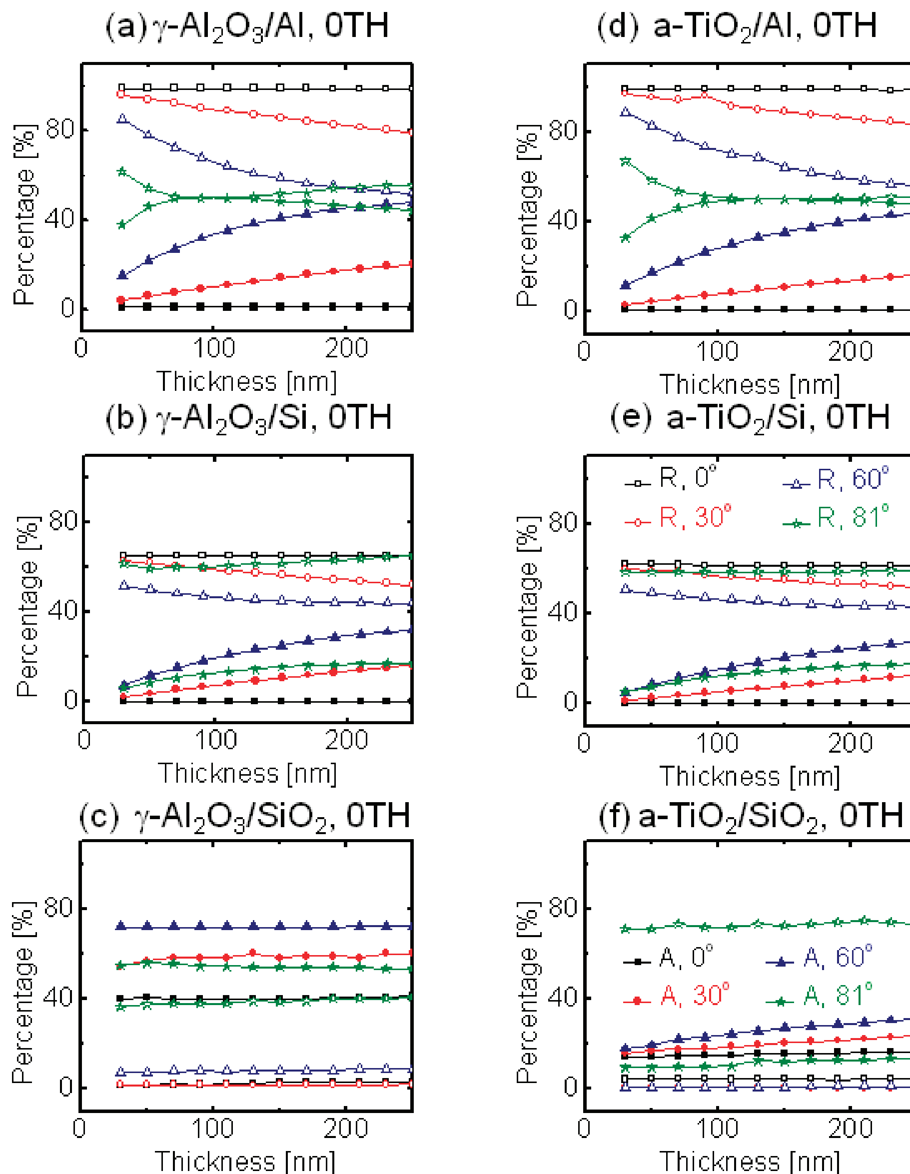

FIG. 8. Same as Fig. 7, zoomed into the oxide film thickness range between 30 and 250 nm.

University College of Science and Mathematics. The authors acknowledge fruitful discussions with Prof. E. A. Vinogradov (Institut of Spectroscopy, Russian Academy of Sciences, Troitsk – Moskow, Russia).

1. K. L. Kliewer and R. Fuchs, Phys. Rev. **144,** 495 (1966).
2. K. L. Kliewer and R. Fuchs, Phys. Rev. **150,** 573 (1966).
3. S. Ghassemi and J. S. Hammonds, Jr., Phys. Lett. A **374,** 4945 (2010).
4. M. Francoeur, R. Vaillon, and M. P. Mengüç, IEEE T. Energy Conver. **26,** 686 (2011).
5. M. Francoeur, M. Pinar Mengüç, and R. Vaillon, Appl. Phys. Lett. **93,** 043109 (2008).
6. S. Shen, A. Narayanaswamy, and G. Chen, Nano Lett. **9,** 2909 (2009).
7. E. Rousseau, A. Siria, G. Jourdan, S. Volz, F. Comin, J. Chevrier, and J.-J. Greffet, Nat. Photonics **3,** 514 (2009).
8. H. Tanaka and K. Hisano, J. Phys.: Condens. Matter **1,** 9539 (1989).
9. E. A. Vinogradov, Phys. Reports **217,** 159 (1992).
10. E. A. Vinogradov, Physics-Uspekhi **45,** 1213 (2002).
11. D. W. Berreman, Phys. Rev. **130,** 2193 (1963).
12. R. Kälin and F. Kneubühl, Infrared Phys. **16,** 491 (1976).
13. S. Mochizuki, Phys. Stat. Sol. B **126,** 105 (1984).
14. G. Scarel, J.-S. Na, and G. N. Parsons, J. Phys. Condens. Matter **22,** 155401 (2010).
15. G. Scarel, J.-S. Na, B. Gong, and G. N. Parsons, Appl. Spectrosc. **64,** 120 (2010).
16. M. Klevenz, S. Wetzel, M. Trieloff, H.-P. Gail, and A. Pucci, Phys. Stat. Sol. B **247,** 2179 (2010).
17. B. C. Trasferetti, C. U. Davanzo, R. A. Zoppi, N. C. da Cruz, and M. A. B. de Moraes, Phys. Rev. B **64,** 125404 (2001).
18. J. Rivnay, L. Jimison, M. F. Toney, M. Preiner, N. A. Melosh, and A. Salleo, J. Vac. Sci. Technol. B **26,** 1454 (2008).
19. F. Comas, H. Calas, and C. Trallero-Giner, Phys. Rev. B **60,** 8238 (1999).
20. G. Scarel, G. K. Hyde, D. Hojo, and G. N. Parsons, J. Appl. Phys. **104,** 094314 (2008).
21. J. S. Ahn, H. S. Choi, and T. W. Noh, Phys. Rev. B **53,** 10310 (1996).
22. V. A. Yakovlv, N. N. Novikova, E. A. Vinogradov, G. Rossetto, A. Sartori, and M. Bolzan, J. Nanopart. Res., February 17 (2011), doi: 10.1007/s1105-011-0280-8
23. G. D. Wilk, R. M. Wallace, and J. M. Anthony, J. Appl. Phys. **89,** 5243 (2001).
24. M. Ritala and M. Leskelä, in *Handbook of Thin Film Materials*, H. S. Nalwa, Ed. (Academic Press, San Diego, CA, 2002), **1**, pp. 103–159.
25. R. Fuchs, K. L. Kliewer, and W. J. Pardee, Phys. Rev. **150,** 589 (1966).
26. W. N. Hansen, J. Opt, Soc. Am. **58,** 380 (1968).
27. D. W. Berreman and F. C. Unterwald, Phys. Rev. **174,** 791 (1968).

28. G. Scarel, C. J. Hirschmugl, V. V. Yakovlev, R. S. Sorbello, C. R. Aita, H. Tanaka, and K. Hisano, J. Appl. Phys. **91,** 1118 (2002).
29. L. Wendler and T. Kraft, Physica B **271,** 33 (1999).
30. H. Welsch and J. Lafait, Opt. Commun. **116,** 369 (1995).
31. M. Załuźny and W. Zietkowski, Physica E **13,** 370 (2002).
32. L. G. Hector and H. L. Schulz, J. Appl. Phys. **7,** 133 (1936).
33. Y. T. Chu, J. B. Bates, C. W. White, and G. C. Farlow, J. Appl. Phys. **64,** 3727 (1988).
34. G. Scarel, C. R. Aita, H. Tanaka, and K. Hisano, J. Non-Cryst. Solids **303,** 50 (2002).
35. R. J. Gonzalez, R. Zallen, and H. Berger, Phys. Rev. B **55,** 7014 (1997).
36. R. D. Kekatpure, E. S. Barnard, W. Cai, and M. L. Brongersma, Phys. Rev. Lett. **104,** 243901 (2010).
37. K. Yamamoto and H. Ishida, Appl. Opt. **34,** 4177 (1995).
38. C. T. Kirk, Phys. Rev. B **38,** 1255 (1988).
39. J. Ibáñez, E. Tarhan, A. K. Ramdas, S. Hernández, R. Cuscó, L. Artús, M. R. Melloch, and M. Hopkinson, Phys. Rev. B **69,** 075314 (2004).
40. G. R. Fowles, *Introduction to Modern Optics* (New York, Dover Publications, 1975), pp. 157.
41. J. D. Jackson, *Classical Electrodynamics* (New York, Wiley, 1999), pp. 310.